Electrocatalysis beyond the reversible hydrogen electrode

Patel, Dipam Manish; Tripathi, Anjana; Ocampo-Restrepo, Vivianne Karina; Kastlunger, Georg

Published in:
Current Opinion in Electrochemistry

Link to article, DOI:
10.1016/j.coelec.2024.101611

Publication date:
2025

Document Version
Publisher's PDF, also known as Version of record

Available online at www.sciencedirect.com

ScienceDirect

Current Opinion in Electrochemistry

Review Article

Electrocatalysis beyond the reversible hydrogen electrode

Dipam Manish Patel, Anjana Tripathi, Vivianne Karina Ocampo-Restrepo and Georg Kastlunger

The reversible and computational hydrogen electrodes have proven invaluable as reference electrodes in aqueous electrocatalysis, allowing an evaluation of the combined chemical potential of the proton–electron pair in experiments and computations. By construction, they cancel the pH dependence in most capacitive processes. However, for electrocatalysis, which is dominated by faradaic processes, this characteristic is rarely observed.

In this short review, we discuss the origins of deviations from the Nernstian behavior in capacitive and faradaic processes, their manifestation in experimental observables, and attempts to incorporate them in simulations. On this basis, we discuss how deviations from Nernstian behavior can be exploited in mechanistic analysis and highlight the use of electrostatic descriptors in computational screening to account for non-Nernstian effects explicitly.

Addresses
Catalysis Theory Center, Department of Physics, Technical University of Denmark (DTU), 2800 Kgs. Lyngby, Denmark

Corresponding author: Kastlunger, Georg (geokast@dtu.dk)

Current Opinion in Electrochemistry 2025, **49**:101611

This review comes from a themed issue on **Fundamental & Theoretical Electrochemistry (2025)**

Edited by **Jan Rossmeisl** and **Henrik Høgh Kristoffersen**

For a complete overview see the Issue and the Editorial

Available online 23 November 2024

https://doi.org/10.1016/j.coelec.2024.101611

Keywords
Electrocatalysis, Computational hydrogen electrode, Non-Nernstian effects, Reversible hydrogen electrode, pH effects, Catalyst screening.

Introduction

The leading characteristic of electrochemistry lies in the fact that electrons and ions are direct reactants or products of half-cell reductions and oxidations. The combined electrochemical potential of a proton in bulk solution and an electron in electrode reservoir, the so-called proton–electron pair, $\tilde{\mu}_{pe} = \tilde{\mu}_p + \tilde{\mu}_e$, is the simplest and by far most relevant "Nernstian couple" in electrocatalysis. Thus, varying it, by means of changing the applied potential and pH is a major driving force, which has been accounted for historically using the potential against the reversible hydrogen electrode (RHE) [1]. Its computational analogue, the computational hydrogen electrode (CHE) model [2], translates RHE potentials to calculated values of $\tilde{\mu}_{pe}$ through the equilibrium between proton–electron pairs and H_2. CHE is essential to account for the major potential effects on $\tilde{\mu}_{pe}$ in simulations and can conveniently be adapted to account for alternative ion–electron pairs being created or annihilated by applying the respective reaction equilibrium potentials and the Nernst equation [3–5].

More recently, the effect of changes in potential and pH beyond purely Nernstian behavior has gathered considerable attention. The source of non-Nernstian behavior has been ascribed to the interaction of varying surface dipoles with an electric field set up by the applied potential [6–8] or changes in the effective number of electrons entering or exiting the investigated system, decoupled from a simultaneous ionic (dis)charge [5,9–12].

Non-Nernstian effects on the formation energy of most adsorbates relevant in electrocatalysis are minor [13]. However, several crucial reaction intermediates have been identified whose energies are susceptive to them [7,13,14]. Furthermore, electrocatalytic activation energies naturally deviate from the Nernstian ideal. In this short review, we discuss how such non-Nernstian effects are expressed in electrocatalytic observables and aim to guide both theoretical and experimental exploration of this variable space. Initially, we outline the role of Nernstian and non-Nernstian effects in capacitive and faradaic processes. We then outline how non-Nernstian effects influence the product selectivity in various electrocatalytic reactions. Finally, we discuss the possibility of including parameters custom to non-Nernstian effects in catalyst screening studies.

Note that a plethora of computational methods for addressing non-Nernstian effects in first principles electrocatalysis are available today [15,16]. We refrain from discussing their details in this article, but rather refer to the respective methodological papers.

RHE/CHE captures most of the potential response in thermodynamics

By construction, the RHE and analogous CHE scales perfectly cancel the pH dependence of processes involving proton discharge or the creation of a proton–electron pair, reducing the number of degrees of freedom from two (absolute electrode potential and proton activity) to one (potential against RHE). Whether this simplification is justified, depends on the nature of the processes under investigation and the elementary steps involved.

A clear distinction can be made between elementary step thermodynamics and kinetics. pH-independence against RHE is generally a reasonable first approximation when exploring the thermodynamic energy landscape within an electrocatalytic process. This independence is reflected by the minor changes in peak positions of water dissociation reactions with pH within cyclic voltammograms (CVs), as shown in Figure 1a. Despite a 12-unit change in pH (corresponding to a shift of 0.7 V vs SHE), the H adsorption region remains static. Notably, the OH adsorption region differs, due to considerable non-Nernstian effects on *OH [18], which will be discussed later. In the absence of such effects, a plethora of theoretical studies have successfully reproduced CV peaks by applying CHE [11,19–22]. We note, however, that detailed shapes of CV peaks and their evolution with varying electrolyte composition (competing ions and buffers) are often poorly captured by this simple approach. This aspect was recently highlighted by Hörmann and Reuter on simulated CVs of capacitive adsorption of halide ions on Ag [5]. The use of a traditional ion reference electrode (denoted as CHE in Figure 1b) produces identical peak shapes across ions (middle row). Only through including non-Nernstian effects, by means of varying charge stored in the (implicitly) simulated electrochemical double-layer (CHE + DL in Figure 1b), can experimental peak shapes be reproduced.

As another example, Rossmeisl et al. explained such a deviation in the peak shapes of the fingerprint region of Pt (111) with varying electrolyte pH by competitive adsorption of alkali cations on the electrode surface. In this model, the reference of both water-based ions and

Figure 1

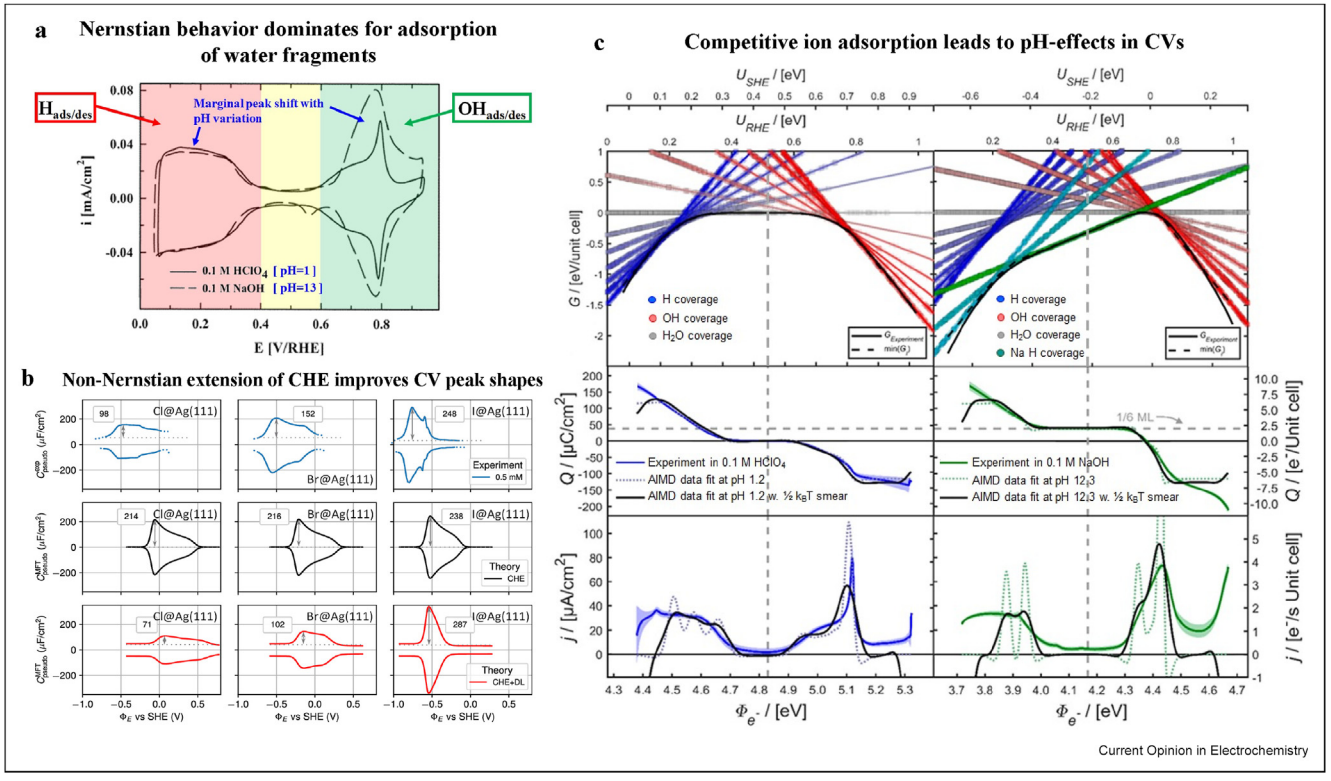

Capacitive processes, based on adsorption equilibria are predominantly Nernstian, as exemplified by the minor influence of pH on the CV peak positions of H/OH adsorption on Pt(111) on the RHE scale, shown in **(a)**. However, non-Nernstian effects can influence peak shapes via electrostatic interactions **(b)** or competitive adsorption **(c)**. **(a)** Adapted with permission from Ref. [17]. Copyright 2001 American Chemical Society **(b)** Reprinted from Ref. [5]. Copyright 2021 American Chemical Society under [CC BY 4.0] [https://creativecommons.org/licenses/by/4.0/] **(c)** Adapted with permission from Ref. [4]. Copyright 2020 American Chemical Society.

sodium in bulk electrolyte is still based on the Nernst equation [4]. However, the (absolute) electrode potential is set up by the Pt-electrolyte interface sampled within ab initio molecular dynamics. This allows a decoupling of $\tilde{\mu}_{pe}$ and referencing back to the RHE scale can be made by adding the configurational entropy contribution of protons ($\ln(10)k_BTpH$) to the absolute potential of the standard hydrogen electrode (SHE). Competitive adsorption of electrolyte species has indeed been concluded to be the source of pH dependence of CVs, with anion adsorption being even more pronounced than the example chosen by Rossmeisl et al. [23–25]

Faradaic processes generally exhibit pH dependence vs RHE

In contrast to capacitive processes, governed by adsorption equilibria, Faradaic processes exhibit pH dependence against RHE by default as their activities are governed by elementary step kinetics [26–31]. To understand this behavior, we first acknowledge that, in the absence of mass transport limitations, the current density of a faradaic process is proportional to the *effective* activation energy $\Delta G^{\ddagger}$ [14], following

$$\log_{10}|j|(U,pH) \propto -\frac{\Delta G^{\ddagger}(U,pH)}{\ln(10)k_BT} \tag{1}$$

Thus, the pH dependence of j on potentials against both SHE (as well as other absolute scales) and RHE can be directly inferred from the change of $\Delta G^{\ddagger}$ on these scales. Against SHE, $\Delta G^{\ddagger}$ takes the form:

$$\begin{aligned}\Delta G^{\ddagger}(U_{SHE},pH) = &\sum^{N_{pe}} \Delta G_{0,i} + \Delta G^{\ddagger}_{0,RLS} \\ &\pm\left[\left(N_{pe}+\beta_{RLS}\right)eU_{SHE}\right. \\ &\left.+\left(N_{pe}+\mathbf{1}\right)\ln(10)k_BTpH\right]\end{aligned} \tag{2}$$

where N_{pe} is the number of PCET steps starting from the resting state of the catalyst (equilibrium coverage state at reaction conditions) up to the RLS and β_{RLS} is the purely non-Nernstian polarization of the transition state relative to the polarization of the resting state [32]. $\Delta G_{0,i}$ and $\Delta G^{\ddagger}_{0,RLS}$ refer to the standard free energy of reaction at pH = 0 and U = 0V vs SHE of the N_{pe} PCET reactions starting from the resting state up to the RLS and the reaction barrier of the RLS, respectively. The ±-symbol represents the opposite sign for reduction (+) and oxidations (−). Finally, the bold addition of 1 in the pH-dependent term only applies to acidic conditions for reductions and alkaline conditions for oxidations [14].

In more intuitive terms, only $\tilde{\mu}_e$, varied with the absolute potential, can affect both the RLS initial and transition states as it enters the enthalpies of the two. $\tilde{\mu}_p$, on the other hand, can only affect the initial or final state free energies as it arises from the configurational entropy of protons (or hydroxides) in bulk solution. Note that in the absence of mass transport limitations, it is independent whether the protons are located close to the surface or not, as their equilibrium with the concentration of protons in the bulk solution defines $\tilde{\mu}_p$. Thus, in relative terms, the activation energy changes with pH only if the initial state is pH-dependent, as shown in Figure 2a. Here, the first-order effects of absolute potential and pH on three representative cases within electrochemical reductions are outlined: 1) the creation of a polarized reaction intermediate (i.e. ion-adsorption with only partial discharge, surface reaction creating or destroying a surface dipole) and PCET steps in 2) neutral/alkaline and 3) acidic media [14]. We note that more detailed effects, relating to changes in the double layer structure are neglected in these analyses, but might be additional sources of non-Nernstian behavior. Among the three cases, only PCET steps in acid exhibit pH dependence on an absolute potential scale, assuming no pre-equilibrated elementary steps.

Unlike in absolute potential scales, all three exhibit pH dependence on the RHE scale. $\Delta G^{\ddagger}$ on the RHE scale takes the form [14]

$$\begin{aligned}\Delta G^{\ddagger}(U_{RHE},pH) = &\sum^{N_{pe}} \Delta G_{0,i} + \Delta G^{\ddagger}_{0,RLS} \\ &\pm\left[\left(N_{pe}+\beta_{RLS}\right)eU_{RHE}\right. \\ &\left.-\left(\beta_{RLS}-\mathbf{1}\right)\ln(10)k_BTpH\right]\end{aligned} \tag{3}$$

Resulting from the fact that RHE, by construction, assumes that the contributions of $\tilde{\mu}_p$ and $\tilde{\mu}_e$ are equal in magnitude. Misalignment of the two at the RLS leads to undercounting or overcounting of the contribution of $\tilde{\mu}_p$ depending on the specific proton donor/acceptor.

From Eqs. (2) and (3), it is evident that the pH dependence of j varies on the RHE and SHE scale. On the absolute SHE scale, the variance of j with pH directly reflects the number of equilibrated elementary steps (N_{pe}) before the RLS, thus SHE shows the purely Nernstian response. pH dependence on the RHE scale, on the other hand, arises purely from non-Nernstian contributions to $\Delta G^{\ddagger}$. Thus, evaluating activity changes with respect to the two reference electrodes allows an independent assessment of the two aspects of electrochemical responses without the need for post-processing of the data. Figure 2b summarizes the pH response of j on the two potential scales at varying conditions.

Figure 2

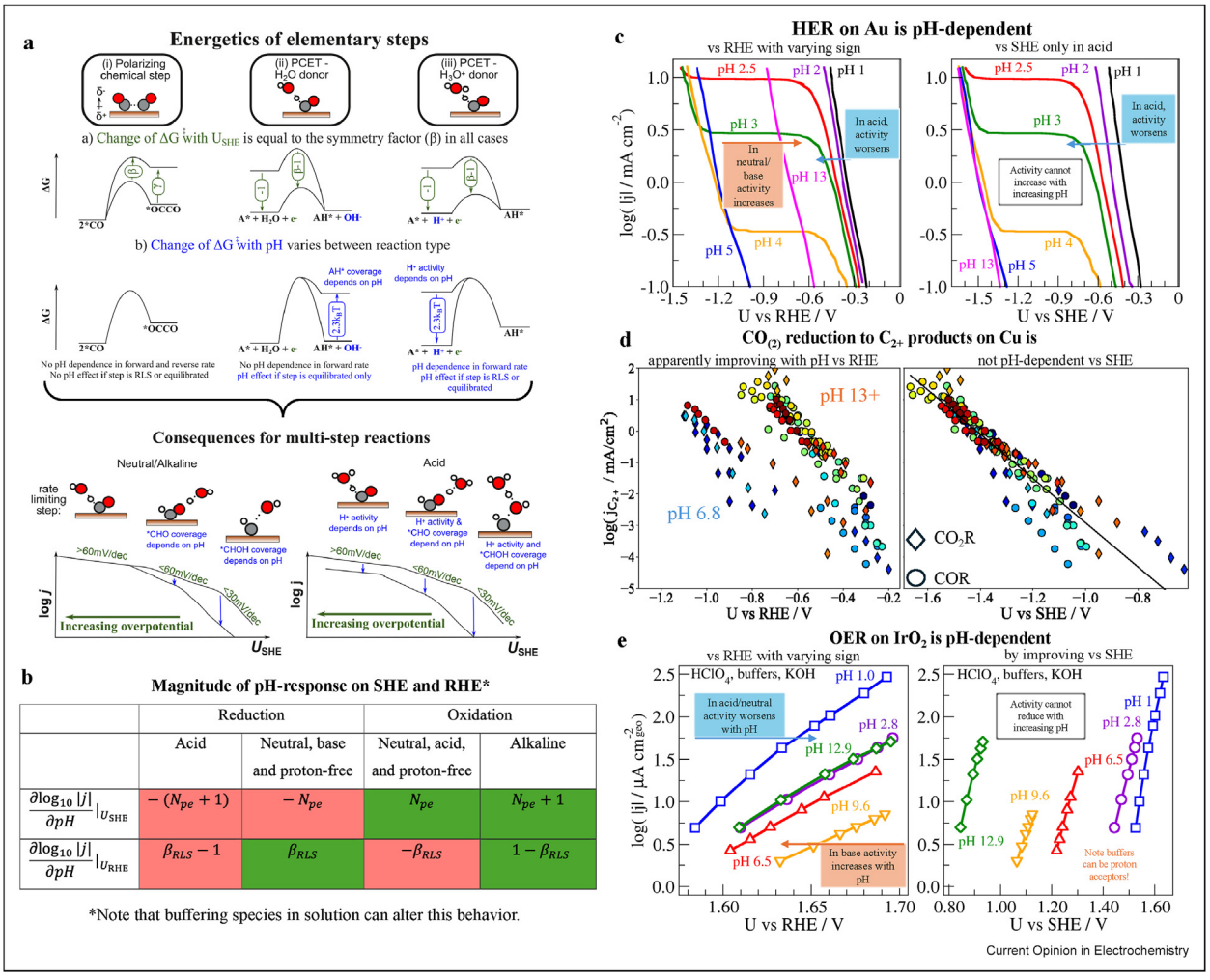

Panel **(a)** highlights the thermodynamic basis for the observed pH dependence, in reduction reactions. Adapted with permission from Ref. [14]. Copyright 2022 American Chemical Society. Magnitude of pH response of faradaic processes against both RHE and SHE is summarized in **(b)**. Reductions limited by a PCET step and a proton-independent RLS are exemplified by **(c)** HER on Au(111) based on experimental data from Ref. [53] and **(d)** $CO_{(2)}$ reduction on Cu, respectively [14]. The behavior of oxidations is exemplified by (e) OER on IrO_2 based on experimental data collected in Ref. [54].

We highlight the pH dependence of faradaic processes in three experimental examples, shown in Figure 2c–e. First, an example of a reduction reaction limited by an initial PCET step, HER on Au, is shown in Figure 2c. As no preceding equilibrated steps occur ($N_{pe} = 0$), j only responds to changes in the initial and transition states of the proton adsorption (Volmer) step. On the RHE scale, this manifests as an apparent increase in activity in neutral/alkaline conditions and a decrease in acidic conditions (see case 3 in Figure 2a). On the absolute SHE scale, activity decreases with increasing pH until leveling out at neutral conditions, where protons are no longer involved in the initial state. On both scales, constant current plateaus occur at intermediate potentials in weakly acidic pHs, indicating proton mass transport is rate-limiting until sufficient potential to make water the proton source.

Figure 2d shows an example of a reaction limited by the formation of a polarized intermediate, $CO_{(2)}$ reduction (COR) to C_{2+} products on Cu. The RLS step here is the dimerization of ∗CO to the strongly polarized $*OCCO^{\delta-}$ (see case 1, Figure 2a). As proton transfer is not involved in this reaction, no pH dependence is observed vs. SHE. On RHE, proton involvement is implicitly assumed, which results in an apparent improvement in activity, due to the negative shift in SHE potential with increasing pH.

As a final example, we showcase the pH dependence of oxidation by considering water oxidation (OER) on IrO_2

in Figure 2e. Note that unlike in Figure 2c, buffers have been used here to alter the magnitude of the pH effects, as they can act as improved proton acceptors compared to water [33]. Nonetheless, the trends are apparent; On the SHE scale, activity can only be pH-independent (acid/neutral without pre-equilibrated steps, water as proton acceptor) or improve (base, OH^- as proton acceptor) with increasing pH. On the other hand, an improvement of activity with pH on the RHE scale is only present in alkaline conditions, while the activity appears to suffer from a pH increase in acidic and neutral media.

The influence of non-Nernstian effects on reaction mechanisms

From all cases described in Figure 2, we can infer that non-Nernstian effects are a central component of catalytic activity and selectivity that is hidden if CHE is not complemented with a non-Nernstian extension. To elaborate on this argument, we show the formation energy of various reaction intermediates at varying interfacial electric fields in Figure 3a [34]. While for most adsorbates the effect of the electric field is minor, some key reaction intermediates (e.g. $*CO_2$, *OCCO, *OH) are very susceptible to the presence of an electric field on the catalyst and, thus, explaining both selectivity and activity of several electrocatalytic reactions necessitates incorporating this effect.

We showcase two theoretical studies on the oxygen reduction reaction (ORR) and COR in Figure 3b and c, respectively, to address the relevance of non-Nernstian effects for mechanistic analysis [8,35]. Figure 3b, shows the effect of the interfacial field, as varied by experiments at constant potential vs RHE but varying pH, on the activity of ORR towards H_2O_2 [6]. Evaluating reaction energies at relevant fields revealed that increasing negative field strength (analogous to increasing pH at a constant RHE potential) increases total (H_2O + H_2O_2) activity on all studied catalyst surfaces. Uniquely, on Au (100), increasing fields decreases the cost of *OOH formation to the point of changing the H_2O_2 RDS to *OOH protonation. As a result, the H_2O_2 activity of Au (100) increases less than expected from the gains of *OOH stabilization. Thus, the H_2O pathway dominates on Au (100), as seen experimentally, unlike Pt (111) and Au (111) where the H_2O_2 RDS remains static and both pathways receive commensurate rate increases with field strength.

The importance of non-Nernstian effects in COR has been identified already in the seminal work of Hori et al. [36,37] Both the RLSs in the reduction of CO_2 to CO on coinage metals [38–40] and CO to C_{2+} products [41] are widely accepted as the formation of highly polarized intermediates [14,42–44]. Figure 3c highlights a recent

Figure 3

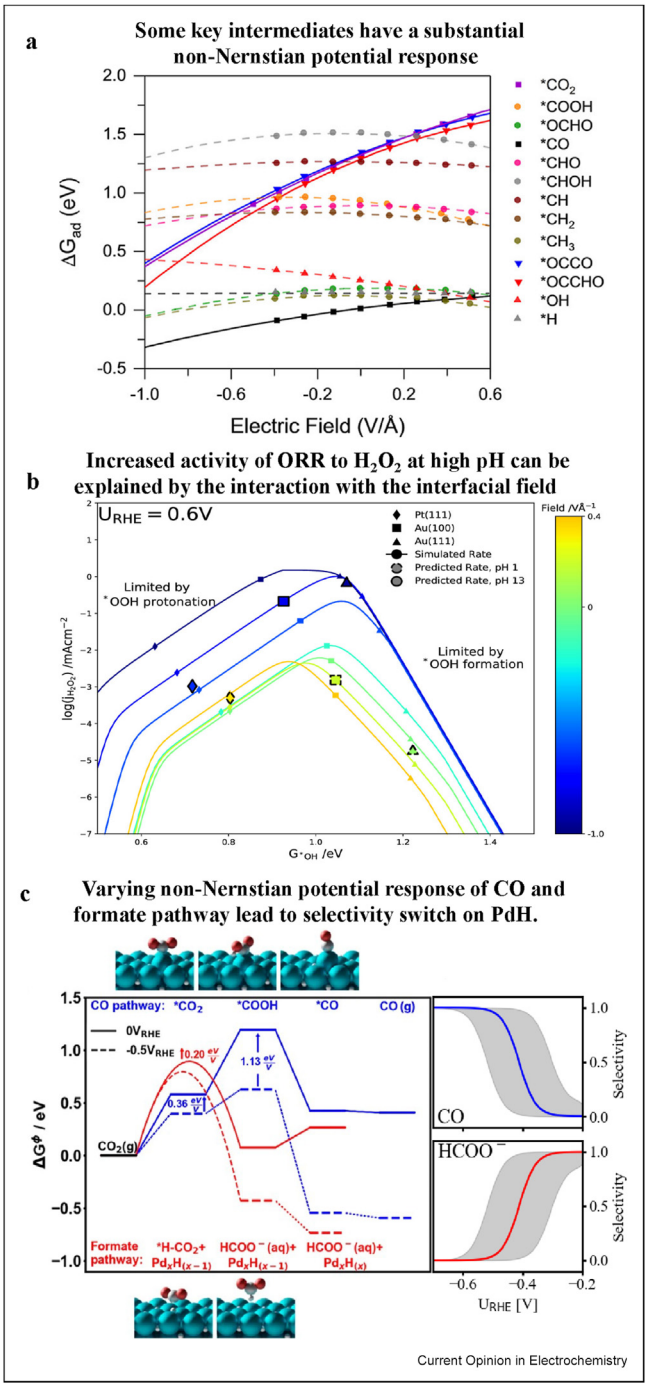

Non-Nernstian potential responses of reaction intermediates and transition states. **(a)** Energy of adsorbates on Cu (111) in response to an applied electric field. Reprinted with permission from Ref. [34]. Copyright 2017 American Chemical Society **(b)** Simulated H_2O_2 activity with varying field strength. Activities of specific catalyst surfaces are shown as points. Reprinted with permission from Ref. [8]. Copyright 2020 American Chemical Society **(c)** Reaction pathway of CO/formate production at varying potential (left) and corresponding selectivity with applied potential (right). Adapted from Ref. [35]. Copyright 2024 Nature under [CC BY 4.0] [https://creativecommons.org/licenses/by/4.0/].

study on the competition of CO and formate selectivity on PdH [35]. Experiments showed that formate is the preferred product down to ∼ -0.4V against RHE, while CO governs at higher overpotentials. An analysis of the kinetics of the respective mechanisms at varying applied potentials suggested that formate production, where CO_2 can be hydrogenated on the C-atom by accepting a hydride H, is kinetically favored at low overpotentials, but the kinetic barrier only marginally responds to changes in the applied potential. On the other hand, the mechanism to CO, where CO_2 adsorbs and undergoes a PCET step protonating the O-atom, benefits substantially from a more cathodic potential.

Non-Nernstian descriptors for catalyst screening

The centrality of non-Nernstian effects in electrocatalysis is further corroborated by the success of correlating field descriptors with catalytic activity. Such correlations between electrostatic quantities and activity have existed since the mid-20th century [45–48], but common practice remains with covalent descriptors, such as binding energies, despite substantial gains in description available with electrostatic descriptors. A recent data-based assessment on electronic structure descriptors for HER by Østergaard et al. highlighted in Figure 4a [49], identified a correlation of catalytic activity with the catalyst work function equal in quality to that with the classical Sabatier principle descriptor of hydrogen binding strength. An analogous first-principles analysis of the reaction barrier within acidic HER conducted by Chen et al. [50], shown in Figure 4b, found that while reaction thermodynamics of the Volmer step do not correlate with its intrinsic barrier, the work function shows a strong correlation with the intrinsic barrier. This result cast doubt on the existence of Brønsted-Ewald-Polanyi relationships in electrocatalysis, a central model in the screening of catalyst materials within thermally activated catalysis.

Recently, Ringe accounted for non-Nernstian effects on the mechanism of COR by applying a 2-dimensional correlation to the reaction selectivity [51]. While the selectivity between producing C_{2+} and CO could be explained by correlating the CO and H binding

Figure 4

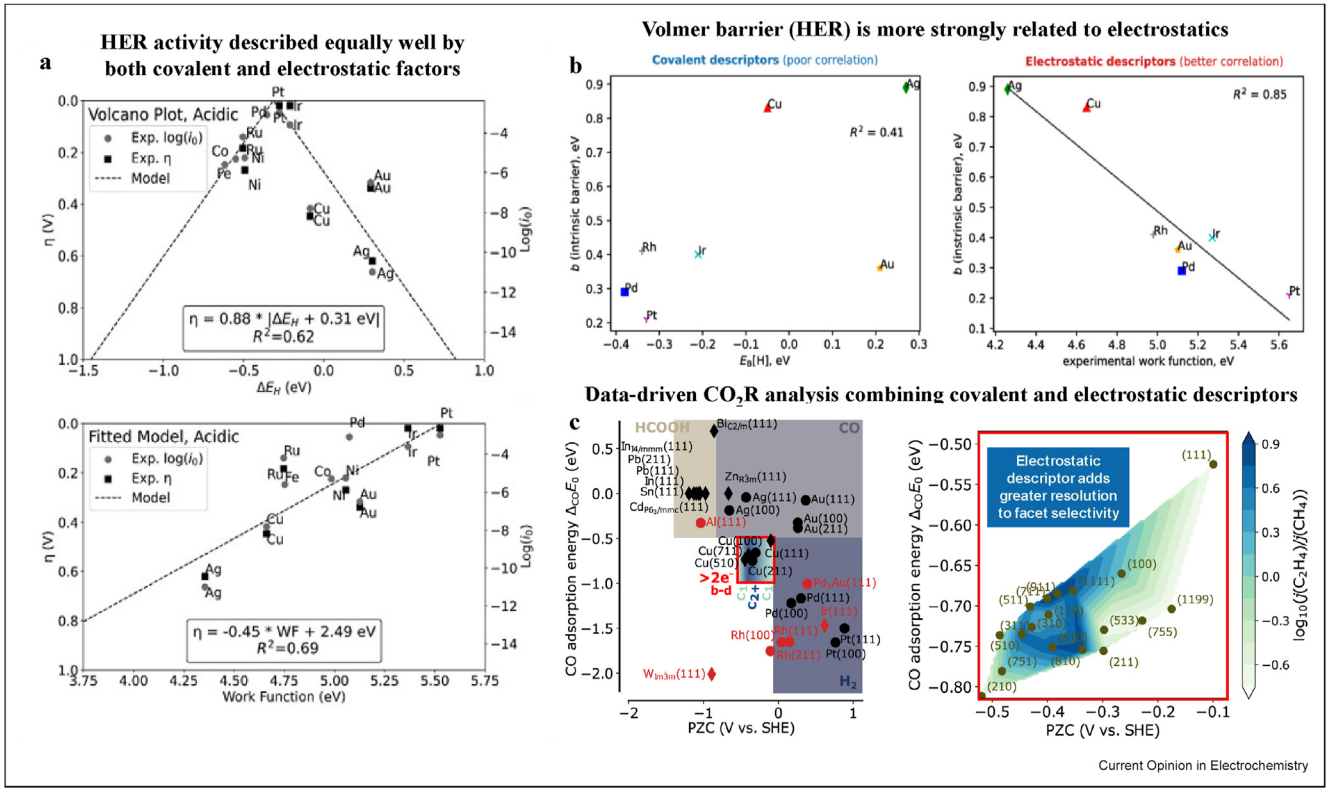

Correlations of activity with simple material descriptors addressing both Nernstian and non-Nernstian contributions to the activity. **(a)** Correlation of measured HER onset potentials, η, with the hydrogen binding strength (top) and work function (bottom). **(b)** Poor correlation of calculated intrinsic reaction barriers, the barrier at the absolute potential of thermoneutral hydrogen binding, of the Volmer reaction with the hydrogen binding strength (left) and superior correlation with the experimental work function (right). **(c)** Selectivity classification for COR based on a combination of a covalent and an electrostatic descriptor. Plots adapted **(a)** from Ref. [49]. Copyright 2022 Elsevier under [CC-BY-4.0] [https://creativecommons.org/licenses/by/4.0/] **(b)** with permission from Ref. [50]. Copyright 2023 American Physical Society **(c)** from Ref. [51]. Copyright 2023 Nature under [CC-BY-4.0] [https://creativecommons.org/licenses/by/4.0/].

strengths [52], the fact that the two descriptors are connected via scaling relations effectively reduces the degrees of freedom to one. On the other hand, the Potential of Zero Charge (PZC) represents a descriptor uncorrelated with CO binding strength, which creates two independent degrees of freedom. This analysis, reproduced in Figure 3c, not only allows for a segregation of products between metals (left), but also a fine resolution of selectivities between metal facets (right). While this study used the theoretical PZC across the same conditions, we note that caution should be paid towards universal application of the PZC, as it is dependent on the electrolyte and often not well defined in experiments.

Conclusion

In electrocatalysis, non-Nernstian effects on thermodynamics and kinetics are ubiquitous. The former are often well simulated by applying CHE, which assumes equal contribution of proton and electron chemical potentials to reaction energetics; however, treatment of kinetics necessitates specific accounting for purely electronic polarization effects, which are most easily observed in the omnipresent pH dependence of faradaic processes against the RHE scale.

Accounting for non-Nernstian contributions is essential to understand product selectivity as highlighted in several landmark electrocatalytic reactions, such as ORR and COR. Consideration of these effects through non-Nernstian descriptors in theoretical screening studies can add a new dimension to the understanding and design of novel electrocatalysts.

Given the plethora of developed DFT-based schemes for incorporating non-Nernstian effects on the fly, we believe that the time is right for theoretical catalyst screening and mechanistic analyses to advance beyond theoretical limiting potentials by accessing the root of catalytic activity, namely elementary step kinetics.

Declaration of competing interest

The authors declare that they have no known competing financial interests or personal relationships that could have appeared to influence the work reported in this paper.

Acknowledgments

During the work on this manuscript, DMP, AT and VOR received funding from Villum Fonden V-SUSTAIN II (grant no. 54345) and GK acknowledges funding from Novo Nordisk foundation grant 0085735.

References

Papers of particular interest, published within the period of review, have been highlighted as:

* of special interest
** of outstanding interest

1. Jerkiewicz G: **Standard and reversible hydrogen electrodes: theory, design, operation, and applications**. *ACS Catal* 2020, **10**:8409–8417.

2. Nørskov JK, *et al.*: **Origin of the overpotential for oxygen reduction at a fuel-cell cathode**. *J Phys Chem B* 2004, **108**: 17886–17892.

3. Koper MTM: **Theory of multiple proton–electron transfer reactions and its implications for electrocatalysis**. *Chem Sci* 2013, **4**:2710.

4. Rossmeisl J, *et al.*: **Realistic cyclic voltammograms from ab initio simulations in alkaline and acidic electrolytes**. *J Phys Chem C* 2020, **124**:20055–20065.

5. * Hörmann NG, Reuter K: **Thermodynamic cyclic voltammograms based on ab initio calculations: Ag(111) in halide-containing solutions**. *J Chem Theor Comput* 2021, **17**: 1782–1794.
Theoretical study showing the interfacial electric field must be included to derive CV peak shapes of halide ion adsorption on Ag (111).

6. ** Dudzinski AM, Diesen E, Heenen HH, Bukas VJ, Reuter K: **First step of the oxygen reduction reaction on Au(111): a computational study of O_2 adsorption at the electrified metal/water interface**. *ACS Catal* 2023, **13**:12074–12081.
A theoretical study showing an example of a non-PCET step being influenced by the applied potential due to dipole-electric field interactions, which cannot be modeled using classical CHE.

7. Vijay S, *et al.*: **Dipole-field interactions determine the CO_2 reduction activity of 2D Fe–N–C single-atom catalysts**. *ACS Catal* 2020, **10**:7826–7835.

8. Kelly SR, Kirk C, Chan K, Nørskov JK: **Electric field effects in oxygen reduction kinetics: rationalizing pH dependence at the Pt(111), Au(111), and Au(100) electrodes**. *J Phys Chem C* 2020, **124**:14581–14591.

9. Katsounaros I, Chen T, Gewirth AA, Markovic NM, Koper MTM: **Evidence for decoupled electron and proton transfer in the electrochemical oxidation of ammonia on Pt(100)**. *J Phys Chem Lett* 2016, **7**:387–392.

10. Hörmann NG, Marzari N, Reuter K: **Electrosorption at metal surfaces from first principles**. *npj Comput Mater* 2020, **6**: 1–10.

11. Li Y, Janik MJ: **Recent progress on first-principles simulations of voltammograms**. *Curr Opin Electrochem* 2019, **14**: 124–132.

12. McCrum IT, Janik MJ: **pH and alkali cation effects on the Pt cyclic voltammogram explained using density functional theory**. *J Phys Chem C* 2016, **120**:457–471.

13. Kastlunger G, Heenen HH, Govindarajan N: **Combining first-principles kinetics and experimental data to establish guidelines for product selectivity in electrochemical CO_2 reduction**. *ACS Catal* 2023, **13**:5062–5072.

14. ** Kastlunger G, *et al.*: **Using pH dependence to understand mechanisms in electrochemical CO reduction**. *ACS Catal* 2022, **12**:4344–4357.
Joint experimental/theoretical study of CO_2 reduction pathways under varying pH, linking observed activity trends with mechanistic changes. This study showcases the predictive power of models that consider non-Nernstian effects and outlines the theory behind pH/applied potential influence on observed kinetics.

15. Abidi N, Lim KRG, Seh ZW, Steinmann SN: **Atomistic modeling of electrocatalysis: are we there yet?** *WIREs Com Mol Sci* 2021, **11**.

16. Levell Z, *et al.*: **Emerging atomistic modeling methods for heterogeneous electrocatalysis**. *Chem Rev* 2024, **124**: 8620–8656.

17. Schmidt TJ, Stamenkovic V, Attard GA, Markovic NM, Ross PN: **On the behavior of Pt(111)-Bi in acid and alkaline electrolytes**. *Langmuir* 2001, **17**:7613–7619.

18. Verma AM, Laverdure L, Melander MM, Honkala K: **Mechanistic origins of the pH dependency in Au-catalyzed glycerol electro-oxidation: insight from first-principles calculations**. *ACS Catal* 2022, **12**:662–675.

19. Karlberg GS, *et al.*: **Cyclic voltammograms for H on Pt(111) and Pt(100) from first principles**. *Phys Rev Lett* 2007, **99**, 126101.

20. Asiri HA, Anderson AB: **Using gibbs energies to calculate the Pt(111) H upd cyclic voltammogram**. *J Phys Chem C* 2013, **117**:17509–17513.

21. Tiwari A, *et al.*: **Fingerprint voltammograms of copper single crystals under alkaline conditions: a fundamental mechanistic analysis**. *J Phys Chem Lett* 2020, **11**:1450–1455.

22. Rossmeisl J, Karlberg GS, Jaramillo T, Nørskov JK: **Steady state oxygen reduction and cyclic voltammetry**. *Faraday Discuss* 2008, **140**:337–346.

23. * Wuttig A, Ryu J, Surendranath Y: **Electrolyte competition controls surface binding of CO intermediates to CO_2 reduction catalysts**. *J Phys Chem C* 2021, **125**:17042–17050.
Experimental evidence of competitive adsorption of CO with carbonate anions on Cu and water on Au. The former indicates a non-Nernstian dependence on pH as carbonate concentration is tied to OH^- concentration.

24. Hochfilzer D, *et al.*: **Transients in electrochemical CO reduction explained by mass transport of buffers**. *ACS Catal* 2022, **12**:5155–5161.

25. Sebastián-Pascual P, Petersen AS, Bagger A, Rossmeisl J, Escudero-Escribano M: **PH and anion effects on Cu-phosphate interfaces for CO electroreduction**. *ACS Catal* 2021, **11**:1128–1135.

26. Govindarajan N, Xu A, Chan K: **How pH affects electrochemical processes**. *Science* 2022, **375**:379–380 (1979).

27. Xu A, Govindarajan N, Kastlunger G, Vijay S, Chan K: **Theories for electrolyte effects in CO_2 Electroreduction**. *Acc Chem Res* 2022, **55**:495–503.

28. Chan K: **A few basic concepts in electrochemical carbon dioxide reduction**. *Nat Commun* 2020, **11**:1–4. 2020 11:1.

29. Liu X, *et al.*: **Understanding trends in electrochemical carbon dioxide reduction rates**. *Nat Commun* 2017, **8**, 15438.

30. Liu X, *et al.*: **pH effects on the electrochemical reduction of CO_2 towards C_2 products on stepped copper**. *Nat Commun* 2019, **10**:1–10.

31. * Fornaciari JC, *et al.*: **Mechanistic understanding of pH effects on the oxygen evolution reaction**. *Electrochim Acta* 2022, **405**, 139810.
An analysis of OER at varying pH on RHE, showing a change in mechanism from acidic to alkaline in experiment and theory.

32. Guidelli R, *et al.*: **Definition of the transfer coefficient in electrochemistry (IUPAC Recommendations 2014)**. *Pure Appl Chem* 2014, **86**.

33. Jackson MN, Surendranath Y: **Donor-dependent kinetics of interfacial proton-coupled electron transfer**. *J Am Chem Soc* 2016, **138**:3228–3234.

34. Resasco J, *et al.*: **Promoter effects of alkali metal cations on the electrochemical reduction of carbon dioxide**. *J Am Chem Soc* 2017, **139**:11277–11287.

35. Abdellah AM, *et al.*: **Impact of palladium/palladium hydride conversion on electrochemical CO_2 reduction via in-situ transmission electron microscopy and diffraction**. *Nat Commun* 2024, **15**:1–15. 2024 15:1.

36. Hori Y: **Electrochemical CO_2 reduction on metal electrodes**. In *Modern aspects of electrochemistry*. New York, NY: Springer New York; 2008:89–189, https://doi.org/10.1007/978-0-387-49489-0_3.

37. Murata A, Hori Y: **Product selectivity affected by cationic species in electrochemical reduction of CO_2 and CO at a Cu electrode**. *Bull Chem Soc Jpn* 1991, **64**:123–127.

38. Hori Y: **Electrochemical CO_2 reduction on metal electrodes**. In *Modern aspects of electrochemistry*, vol. 42. New York, NY: Springer New York; 2008:89–189.

39. Dong Q, Zhang X, He D, Lang C, Wang D: **Role of H_2O in CO_2 electrochemical reduction as studied in a water-in-salt system**. *ACS Cent Sci* 2019, **5**:1461–1467.

40. Cheng T, Xiao H, Goddard WA: **Reaction mechanisms for the electrochemical reduction of CO_2 to CO and formate on the Cu(100) surface at 298 K from quantum mechanics free energy calculations with explicit water**. *J Am Chem Soc* 2016, **138**:13802–13805.

41. Kortlever R, Shen J, Schouten KJP, Calle-Vallejo F, Koper MTM: **Catalysts and reaction pathways for the electrochemical reduction of carbon dioxide**. *J Phys Chem Lett* 2015, **6**:4073–4082.

42. Resasco J, Bell AT: **Electrocatalytic CO_2 reduction to fuels: progress and opportunities**. *Trends Chem* 2020, **2**:825–836.

43. Hussain G, *et al.*: **How cations determine the interfacial potential profile: relevance for the CO_2 reduction reaction**. *Electrochim Acta* 2019, **327**.

44. Vijay S, *et al.*: **Unified mechanistic understanding of CO_2 reduction to CO on transition metal and single atom catalysts**. *Nat Catal* 2021, **4**:1024–1031.

45. Bockris JOM: **Electrolytic polarisation—I. The overpotential of hydrogen on some less common metals at high current densities. Influence of current density and time**. *Trans Faraday Soc* 1947, **43**:417–429.

46. Conway BE, O'M Bockris J: **Electrolytic hydrogen evolution kinetics and its relation to the electronic and adsorptive properties of the metal**. *J Chem Phys* 1957, **26**:532–541.

47. Kita H: **Periodic variation of exchange current density of hydrogen electrode reaction with atomic number and reaction mechanism**. *J Electrochem Soc* 1966, **113**:1095.

48. Trasatti S: **Work function, electronegativity, and electrochemical behaviour of metals: III. Electrolytic hydrogen evolution in acid solutions**. *J Electroanal Chem Interfacial Electrochem* 1972, **39**:163–184.

49. Østergaard FC, Bagger A, Rossmeisl J: **Predicting catalytic activity in hydrogen evolution reaction**. *Curr Opin Electrochem* 2022, **35**, 101037.

50. Chen X, Kastlunger G, Peterson AA: **Fundamental drivers of electrochemical barriers**. *Phys Rev Lett* 2023, **131**, 238003.

51. ** Ringe S: **The importance of a charge transfer descriptor for screening potential CO_2 reduction electrocatalysts**. *Nat Commun* 2023, **14**:1–14. 2023 14:1.
A two-dimensional, covalent and electrostatic, descriptor analysis of CO_2 reduction catalysts explains trends in product selectivity and establishes a basis for breaking scaling relations through PZC-informed catalyst design.

52. Bagger A, Ju W, Varela AS, Strasser P, Rossmeisl J: **Electrochemical CO_2 reduction: a classification problem**. *ChemPhysChem* 2017, **18**:3266–3273.

53. Strmcnik D, *et al.*: **Improving the hydrogen oxidation reaction rate by promotion of hydroxyl adsorption**. *Nat Chem* 2013, **5**:300–306.

54. Kuo DY, *et al.*: **Influence of surface adsorption on the oxygen evolution reaction on IrO2(110)**. *J Am Chem Soc* 2017, **139**:3473–3479.